Modern Journal of Health and Applied Sciences *(MJHAS)*
E-ISSN 3078-2791; P-ISSN 3078-2783
Journal homepage: https://mucjournals.muc.edu.ps

A new approach for studying plaster beam bending based on DISS Algerian (nano-short-bio-fibres)

Abdelmoutalib Benfrid [1,2*], *and Mohamed Bachir Bouiadjra* [1,2]

[1] Laboratory of Advanced Structures and Materials in Civil Engineering and Public Works, University of Djillali Liabes, 22000 Sidi Bel-Abbes, Algeria.
[2] Thematic Agency for Research in Science and Technology, ATRST, 16000 Algiers, Algeria.

ARTICLE INFO

Received: 12th November 2024
Received in revised form: 21th December 2024
Accepted: 25th December 2024
Published: 15th March 2025

***Corresponding Author:**
Abdelmoutalib Benfrid
E-mail:
benfridabdelmoutalib2050@gmail.com

Citation: Benfrid, A., & Bachir Bouiadjra, M. A new approach for studying plaster beam bending based on DISS Algerian (nano-short-bio-fibres). *Modern Journal of Health and Applied Sciences*, 2(1), 43-58.

DOI: https://doi.org/10.70411/MJHAS.2.1.2025183

ABSTRACT

Construction materials, particularly plaster (gips), are crucial in civil engineering and architecture. Due to their durability, it is essential to use durable materials. A Berber plant, a renewable and persistent plant, has been chosen to improve the mechanical properties of plaster (gips). The PIGGOT rule of homogenization was used to determine the properties of the total set, with plaster as the matrix and DISS (Scrip) as the reinforcement. A high-order mathematical model was established to study the bending of a new bio-beam using local materials, resulting in the birth of the beam. The results show that the deflection of the bio-plaster beam decreases with an increase in the nano-short-fibre fraction of DISS (Scrip). The main objective is to reinforce plaster and reduce flexion by utilizing the effect of short fibres to enhance shear performance. Another goal is to minimize the flexion of plaster beams. Additionally, this approach aims to introduce innovation in the field of construction and civil engineering while promoting the use of biological substitutes in this sector. This study will be conducted analytically through homogenization and analysing the non-local flexure of beams rather than experimentally.

Keywords: The plaster, Mechanical properties, PIGGOT (homogenization), Deflexion, Bio-beam.

.

1. Introduction

Plaster (gips) is a traditional construction material that consolidates in water, taking various forms such as beams, plates, and panels. It is also used as a wall coating or bonding agent between bricks in masonry. Recently, significant progress has been made in improving this material, with several studies exploring its properties and performance. Plaster is obtained by dehydrating gypsum ($CaSO_4 \cdot 2H_2O$), a hydrated calcium sulfate, to form anhydrite ($CaSO_4$). In recent research, experimental results have studied and validated steel-reinforced plaster boards for paving structures, though adjustments may be necessary depending on reinforcement or anchoring configurations (Karni & Karni, 1995). Plaster coatings with lightweight aggregates impregnated with phase-change materials (PCM) have significantly reduced building energy consumption, with maximum savings of 293.8 kWh (Wadee et al., 2023; Wang et al., 2023). Adding recycled plastic and glass to plaster coatings has increased the strength and density of plaster beams, improving their brittle behaviour (Boukert et al., 2019). Furthermore, research on lime-based plasters has demonstrated high compressive strength and proposed mathematical models to predict their behaviour (Abdullah & Sichani, 2009; Rahimzadeh et al., 2022). Flash calcination of gypsum has led to the development of new plaster composite particles with unique properties, such as maintaining γ-anhydrite in humid conditions, unlike traditional plaster (Berenger et al., 2015). Studies have shown significant strength loss above 500°C for plaster exposed to high temperatures, with complete loss of strength for some plaster types at higher temperatures (Mohammed, 2010; Yaqoob, 2019). Incorporating recycled materials like PET and sawdust into lightweight plaster boards has yielded optimal thermal insulation and mechanical strength (Ali et al., 2015). Adding kaolin and metakaolin has also shown positive effects, increasing the compressive strength of plaster (Fahih et al., 2005). In addition, polymer coatings have improved the strength of plaster beams, reducing the risk of rupture under high loads (Saurav & Porter, 2018). On the theoretical side, non-local continuum theories, such as Eringen's non-local elasticity theory, have been used to analyse the response of nanostructures, specifically nanobeams, accounting for size effects at the nanoscale (Sayyad & Ghugal, 2021; Sayyad et al., 2023). Higher-order deformation models have been proposed to simulate the behaviour of plaster beams reinforced with short fibres, using Piggot's homogenisation rule to treat these materials as isotropic. Timoshenko's works have validated this model. Timoshenko has many statistical studies that address the issue of flexure (Timoshenko & Gere, 2012). Arbabi improves methods through non-local analysis by enhancing the Timoshenko model (Arbabi, 1991) and forms the basis of this study on the bending behaviour of plaster beams, validated by a mathematical model with advanced deformation functions and homogenisation via Piggot (Sayyad & Ghugal, 2021; Sayyad et al., 2023). It is noted that the plaster and gypsum are the exact definition, but the **DISS** is a plant material often found in regions bordering the Mediterranean. This Berberian plant grows in the Berber world, which signifies a random world. The word "Berber" comes from the language of the Algerian population and refers to a forest plant. This study focuses on non-local flexure but does not address long-term control or durability effects. The idea stems from ancient constructions in the Bous region, where this plant was frequently used in old buildings. For this reason, the goal is to analyse the non-local effect on plaster beams, considering the adhesion between fibres and plaster particles, which generates a significant shear effect.

2. Model Mathematics

2. 1. Homogenization

The Piggot rule (Piggott, 1981; Piggott, 2002) for homogenisation remains highly relevant and is still utilised for homogenising materials reinforced with short fibres, despite the advancements made in the works of (TKAYANAGI 1 & 2) (Jamalzadeh et al., 2018; Zare & Rhee, 2020). Recent studies, such as those by (MARIANNA RINALDI et al.) (Rinaldi et al., 2023), have applied the original Piggot rule to investigate the performance of a 3D-printed material made from polyether-ether-ketone (PEEK) reinforced with short carbon nanotube fibres (nano short fibres of CNTs). This highlights the continued validity of the Piggot rule up to 2023. However, it is important to note that the theory's applicability assumes that the matrix material is relatively weak. The difference in the elastic properties between the matrix and the reinforcement is insignificant, making the rule applicable in such scenarios. When ζ_d is the ratio between the maximum fibre diameter and the particles diameters of the ultimate plaster grains, and λ_l is the ratio between the maximum fibre length and the minimum length fibre of the reinforcing fibres. $E_{\text{hom}}^{P\&D}$ is the module of young homogeneous. $E_P ; E_D$ are the module of young of Plaster and the DISS respectively, $\upsilon_{\text{hom}}^{P\&D} ; \nu_P ; \nu_D$ are the ratio Poisson of homogeneous, Plaster and the DISS respectively and the same goes for other factors, such as volume fraction V_D and shear modulus $G_{\text{hom}}^{P\&D}$.

$$E_{\text{hom}}^{P\&D} = (\frac{1}{5} V_D \times \zeta_d \times \lambda_l \times E_D) + (V_P \times E_P) ....(a)$$

$$\zeta_d = \frac{D_{f\,\max}^D}{D_{p\,\max}^P} ...(b)....... \lambda_l == \frac{L_{f\,\max}^D}{L_{f\,\min}^D} ....(c)...... V_P + V_D = 1....(d) \qquad \text{Eq.01}$$

$$\upsilon_{\text{hom}}^{P\&D} = \nu_P \times V_P + \nu_D \times V_D ....(e)...... G_{\text{hom}}^{P\&D} = \frac{E_{\text{hom}}^{P\&D}}{2(1+\upsilon_{\text{hom}}^{P\&D})} ....(f)$$

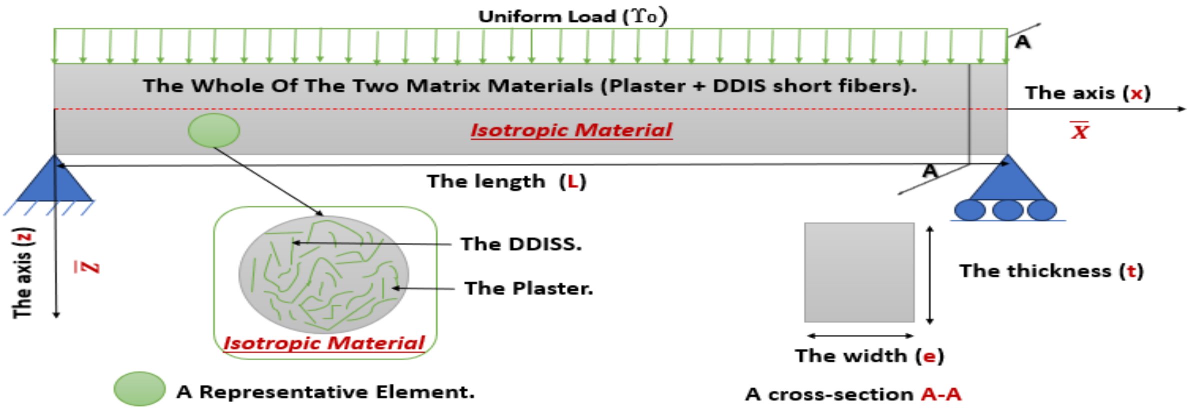

Figure 1. Presentation of the beam is considered isotropic (Plaster reinforced by the nano-short fibers) with uniform loading.

2. 2. Bending beam

The kinematics of isotropic beam is written as presented below:

$$\overline{X}(x,z,d) = \overline{x_0}(x,d) - z \times \frac{\partial \overline{z_0}}{\partial x} + \chi(z) \times \psi(x,d) .... \overline{Z}(x,z,d) = \overline{z_0}(x,d). \qquad \text{Eq.02}$$

$\overline{X}$ and $\overline{Z}$ are the axial and transverse displacement respectively in x and z directions where the x axis confused on the neutral axis), and ψ is the shear slope. $\overline{x_0}$ and $\overline{z_0}$ are the displacement in any position.

$$\Omega_x = \frac{\partial \overline{Z}}{\partial x} = \Omega_x^0 + z \times \mathrm{P}_x^b + \chi(z) \times \mathrm{P}_x^s. \qquad \text{Eq.03}$$

$$\wp_{xz} = \frac{\partial \overline{Z}}{\partial z} + \frac{\partial \overline{X}}{\partial x} = \delta(z) \times \wp_{xz}^0.$$

Where:

$$\Omega_x^0 = \frac{\partial \overline{x_0}}{\partial x} ; \mathrm{P}_x^b = -\frac{\partial^2 \overline{x_0}}{\partial x^2} ; \mathrm{P}_x^s = \frac{\partial \psi}{\partial x} ; \wp_{xz}^0 = \psi.$$

$$\chi(z) = \frac{3}{8} \times z + \frac{41 \times z^3}{30 \times t^2} - \frac{1}{2} \times t \times \arctan(\frac{z}{t}). \qquad \text{Eq.04}$$

$$\delta(z) = 1 - \frac{\partial \chi(z)}{\partial z}.$$

For the bending of a beam, the normal and the tangential stress are as follows:

$$\sigma_x = E_{\text{hom}}^{P\&D} \times (\Omega_x^0 + z \times \mathrm{P}_x^b + \mathrm{P}_x^s \times \chi(z)) \ldots\ldots\ldots\ldots \tau_{xz} = \frac{E_{\text{hom}}^{P\&D}}{2 \times (1 + \upsilon_{\text{hom}}^{P\&D})} \times \delta(z) \times \wp_{xz}^0 . \qquad \text{Eq.05}$$

Where $E_{\text{hom}}^{P\&D}$ and $\upsilon_{\text{hom}}^{P\&D}$ are the elastic modulus and Poisson's ratio of a homogeneous plaster beam reinforced by short DISS fibres are determined after homogenization as an isotropic beam.

Hamilton's principle determines equilibrium equations, considering the initial during (**d_i**) and the final during (**d_f**).

$$\int_{d_i}^{d_f} (\delta \mathrm{H} - \delta \mathrm{P}) dt = 0 \ldots\ldots\ldots\ldots \delta \mathrm{H} = e \int_0^L \int_{-\frac{t}{2}}^{\frac{t}{2}} (\sigma_x \delta \Omega_x + \tau_{xz} \delta \wp_{xz}) dz dx.$$

$$\delta \mathrm{H} = \int_0^L (F_r^x \delta \Omega_x^0 + M_r^b \delta \mathrm{P}_x^b - M_r^s \delta \mathrm{P}_x^s + \Re' \wp_{xz}^0) \ldots\ldots\ldots \delta \mathrm{P} = \int_0^L (\Upsilon(x) \delta w) dx. \qquad \text{Eq.06}$$

We note that $\Upsilon(x)$ is the loading applied to the beam studied. $(F_r^x ; M_r^b ; M_r^s ; \Re')$ are the resulting forces and moments obtained by the thickness (z= { $-\frac{t}{2}$ to $\frac{t}{2}$ }).

$$F_r^x = e \int_{\frac{-t}{2}}^{\frac{t}{2}} 1 \times \sigma_x dz = \bar{A}_{st} \times \Omega_x^0 + \bar{B}_{st} \times z \times \mathrm{P}_x^b + \bar{C}_{st} \times \mathrm{P}_x^s \times \chi(z) \ldots\ldots\ldots\ldots\ldots\ldots M_r^b = e \int_{\frac{-t}{2}}^{\frac{t}{2}} z \times \sigma_x dz = \bar{B}_{st} \times \Omega_x^0 + \bar{C}_{st} \times z \times \mathrm{P}_x^b + \bar{E}_{st} \times \mathrm{P}_x^s \times \chi(z).$$

$$M_r^s = e \int_{\frac{-t}{2}}^{\frac{t}{2}} z \times \chi(x) \times \sigma_x dz = \bar{C}_{st} \times \Omega_x^0 + \bar{E}_{st} \times z \times \mathrm{P}_x^b + \bar{F}_{st} \times \mathrm{P}_x^s \times \chi(z) \ldots\ldots \Re' = e \int_{\frac{-t}{2}}^{\frac{t}{2}} \delta(x) \times \tau_{xy} dz = \bar{G}_{st} \times \wp_{xz}^0 . \qquad \text{Eq.07}$$

$(\bar{A}_{st} ; \bar{B}_{st} ; \bar{C}_{st} ; \bar{D}_{st} ; \bar{E}_{st} ; \bar{F}_{st} ; \bar{G}_{st})$ are the stiffness coefficients; where:

$$\bar{A}_{st} = e \int_{\frac{-t}{2}}^{\frac{t}{2}} 1 \times E_{\text{hom}}^{P\&D} dz \ldots\ldots\ldots\ldots\ldots\ldots\ldots \bar{B}_{st} = e \int_{\frac{-t}{2}}^{\frac{t}{2}} z \times E_{\text{hom}}^{P\&D} dz.$$

$$\bar{C}_{st} = e \int_{\frac{-t}{2}}^{\frac{t}{2}} \chi(z) \times E_{\text{hom}}^{P\&D} dz \ldots\ldots\ldots\ldots \bar{D}_{st} = e \int_{\frac{-t}{2}}^{\frac{t}{2}} z^2 \times E_{\text{hom}}^{P\&D} dz.$$

$$\bar{E}_{st} = e \int_{\frac{-t}{2}}^{\frac{t}{2}} z \times \chi(z) \times E_{\text{hom}}^{P\&D} dz \ldots\ldots \bar{F}_{st} = e \int_{\frac{-t}{2}}^{\frac{t}{2}} \chi^2(z) \times E_{\text{hom}}^{P\&D} dz. \qquad \text{Eq.08}$$

$$\bar{G}_{st} = e \int_{\frac{-t}{2}}^{\frac{t}{2}} \delta^2(z) \times E_{\text{hom}}^{P\&D} dz.$$

We replace equations N° (7 and 8) into equation N°(6) and replace all the parameters. To obtain the equilibrium equations, we find the following:

$$\delta\overline{x_0}:\frac{\partial F_r^x}{\partial x}=0..................\delta\overline{x_0}:\bar{A}\frac{\partial^2\overline{x_0}}{\partial x^2}-\bar{B}\frac{\partial^3\overline{z_0}}{\partial x^3}+\bar{C}\frac{\partial^2\psi}{\partial x^2}=0.$$

$$\delta\overline{z_0}:\frac{\partial M_r^b}{\partial x^2}+\Upsilon=0...........\delta\overline{z_0}:-\bar{B}\frac{\partial^3\overline{x_0}}{\partial x^3}+\bar{D}\frac{\partial^3\overline{z_0}}{\partial x^3}-\bar{E}\frac{\partial^3\psi}{\partial x^3}+\Upsilon(x)=0. \quad \text{Eq.09}$$

$$\delta\psi:\frac{\partial M_r^s}{\partial x}-\Re^{'}=0...........\delta\psi:\bar{C}\frac{\partial^2\overline{x_0}}{\partial x^2}-\bar{E}\frac{\partial^3\overline{z_0}}{\partial x^3}+\bar{F}\frac{\partial^2\overline{\psi}}{\partial x^2}+\bar{G}\times\psi=0.$$

Applying the boundary conditions of a beam supports when **x=0** and **x=L**.

$$\overline{x_0}=\overline{Z}=M_r^b=M_r^s=0. \quad \text{Eq.10}$$

We are utilizing Navier solutions to address the issue, as they are outlined in the following:

$$\overline{x_0}=\sum_{m=1,3,5}^{\infty}x_m\times\cos(\varsigma\times x)...........\overline{z_0}=\sum_{m=1,3,5}^{\infty}z_m\times\sin(\varsigma\times x). \quad \text{Eq.11}$$

$$\psi=\sum_{m=1,3,5}^{\infty}\psi_m\times\cos(\varsigma\times x)...........\Upsilon(x)=\sum_{m=1,3,5}^{\infty}\frac{4\times\Upsilon_0}{m\times\pi}\times\sin(\varsigma\times x).$$

The Υ_0 is the maximum uniform load; using the relation rigidity displacement equal to the force generated to determine the deflection (z_m) ; With [$\mathbf{K_r}$] as the rigidity matrix, {$\mathbf{U_d}$} as the displacement vector, and {$\mathbf{P_r}$}as the force vector; when (**œ**) the parameter is non-local and cogent the characteristics of materials used in analyses, it's noted that (**n**) written with this formula {$\mathbf{n=(k_0\times œ)^2}$}; noting the next relation matrix to solve the problems and calculate the deflexion $\overline{\overline{Z_{adm}}}$:

$$\{P_r\}=[K_r]\times\{U_d\}. \quad \text{Eq.12}$$

Let's define the last matrix of rigidity [**Kr**], force {**Pr**} and displacement {**Ud**}.

$$[K_r]=\begin{bmatrix}\bar{A}\times\varsigma^2 & -\bar{B}\times\varsigma^3 & \bar{C}\times\varsigma^2\\ -\bar{B}\times\varsigma^3 & D\times\varsigma^4 & -\bar{E}\times\varsigma^3\\ \bar{C}\times\varsigma^2 & -\bar{E}\times\varsigma^3 & \bar{F}\times\varsigma^2+\bar{G}\end{bmatrix}....\{U_d\}=\begin{Bmatrix}x_m\\ z_m\\ \psi_m\end{Bmatrix}. \quad \text{Eq.13}$$

$$\{P_r\}=\frac{4\times\Upsilon_0}{m\times\pi}\begin{Bmatrix}0\\ (1+n\varsigma^2\\ 0\end{Bmatrix}........................\varsigma=\frac{m\times\pi}{L}.$$

The dimensionless deflection is written in following:

$$\overline{\overline{Z_{adm}}}=100\times\frac{E_P}{\Upsilon_0\times L^4}\times\frac{e\times t^3}{12}. \quad \text{Eq.14}$$

3. Results and discussion

3. 1. Model of homogenization Comparison

At first, to validate that the young model is valid by the developed model, we compare the results by the reference of (Marianna Rinaldi) (Rinaldi et al., 2023) with the diameter of CNTs **(dcnt =06 nm)** in **Table 1,** where (**$\mathbf{E_{polymere}}$.=3 GPA; $\mathbf{n_{polymere}}$ =0.3**) and the nanotube of carbon reinforced are (**$\mathbf{E_{CNTs}}$ = 5.6466 TPa, $\mathbf{v_{CNTs}}$ =0.34**). You can see the error between the real modulus of elasticity and the effective modulus of elasticity when the matrix is the polymer and the fibres reinforced are the

CNTs when the units are **[GPa]**. The error will be presented as a percentage [**%**] under the following formula:

$$\Delta_{error(\%)} = \frac{E_{piggot} - E_{real}}{E_{real}} \quad \text{Eq.15}$$

Table 1. Model of homogenization Comparison by Model created and with other results from other scientific journals.

	$E_{measured}$	(Marianna Rinaldi) (Rinaldi et al., 2023)		(Jamalzadeh N and al ….) (Jamalzadeh et al., 2018)		(Zare Y and al…) (Zare & Rhee, 2020)		**Present**	
V% CNTs	E_{real}	E_{piggot} **Eq 1**	$\Delta_{error(\%)}$ **Eq 16**	E_{piggot} **Eq 1**	$\Delta_{error(\%)}$ **Eq 16**	E_{piggot} **Eq 1**	$\Delta_{error(\%)}$ **Eq 16**	E_{piggot} **Eq 1**	$\Delta_{error(\%)}$ **Eq 16**
0%	3	3	0	3	0	3	0	**3**	**0**
3%	3.1	7.2	132	5.3	70.8	2.97	0.9	**3.195**	**3.064**
5%	3.5	10	186	3.7	5	3.3	7	**3.324**	**-5.028**
10%	3.7	17.2	356	3.4	8	4.1	11	**3.649**	**-1.378**

According to **Table 1**, the uncertainty is between **±5.1%,** which means that our homogenization model is very close to the experimental parts and the theoretical models mentioned in this last table. So, this developed law is valid for homogenizing non-short fibres (de Bilbao et al., 2010). The elastic modulus and Poisson's ratio of the matrix (Plaster) are as follows: (**E =1.75 GPa ;v=0.25**) and (MERZOUD Mouloud and HABITA Mohamed Fouzi) (Merzoud & Habita, 2008),(Lakhemissi Touam and Semcheddine Derfouf) (Touam & Derfouf, 2021), Layth Mohammed and al …) (Mohammed et al., 2015) reinforcement properties of nano short fibre from Algerian DISS are also noted as: (**E =6.7 GPa ;v=0.2**)

Where: $$\zeta_d = \frac{D^D_{f\,\max}}{D^P_{p\,\max}} = \frac{3nm}{5nm}$$

And: $$\lambda_l == \frac{L^D_{f\,\max}}{L^D_{f\,\min}} = \frac{700nm}{250nm}$$

The results are well illustrated in the following **Table 2**. This last table declares and shows that the mechanical properties increase concerning the increase in nano-short fibres of organic reinforcement (Algerian DISS). We were obliged to stop the increase of **30%** in reinforcement in organic materials in cases where organic materials have the role of reinforcement.

Table 2. The effective results of the model created for the homogenization between plaster and nano fibers of Algerian DISS.

(V%) DISS	$E^{P\&D}_{\text{hom}}$	$\upsilon^{P\&D}_{\text{hom}}$	$G^{P\&D}_{\text{hom}}$	**(V%) DISS**	$E^{P\&D}_{\text{hom}}$	$\upsilon^{P\&D}_{\text{hom}}$	$G^{P\&D}_{\text{hom}}$
0% (Matrix)	1.750	0.25	0.7	**0% (Matrix)**	1.750	0.25	0.7
5%	1.897	0.2475	0.7632	**20%**	2.338	0.24	0.9427
10%	2.044	0.245	0.8129	**25%**	2.485	0.2375	1.0040
15%	2.191	0.2425	0.8817	**30%**	2.632	0.235	1.0656

3. 2. Static bending of the beam (plaster reinforced with nano short fibres from DISS Algeria)

Firstly, we note that the results are compared using our mathematical model by comparing two works of Pr. SAYYAD (Sayyad

& Ghugal, 2021; Sayyad et al., 2023), when the material is considered isotropic, where (**E = 1 GPa ;v=0.2**).

Table 3. Comparison of the results obtained by the model created for an isotropic material with recent scientific work in the same context., where (***E = 1 GPa*** ;***v=0.3***) and the geometric parameters (***t=1;e=1×t;L=ℏ ×t***).

$\hbar = \frac{L}{t}$.	Nonlocal parameter (n) (m=100)	The dimensionless deflection $\overline{\overline{Z_{adm}}}$			
		Sayyad &) (Ghugal, 2021	Sayyad et al., 2023 x=2.634	Sayyad et al., 2023 x=1	**Present**
10	0	1.3394	1.3381	1.3345	**1.3394**
	1	1.4675	1.4660	1.4621	**1.4655**
	2	1.5956	1.5940	1.5897	**1.5983**
	3	1.7237	1.7220	1.7173	**1.7364**
	4	1.8517	1.8498	1.8449	**1.8520**

Table 3 shows that the mathematical model for calculating the bending of isotropic beams is similar to the other researchers' results, which means that the new shear estimation function is valid.

In addition, we also compare the results obtained according to non-local parameters; the results are very close to the article by Professor SAYAD. **Table 4** shows the comparison, which means that our beam bending calculation model is very close; therefore, studying the bending of the plaster beam reinforced by DISS is also functional.

The non-linear model varies between 0 to 4. All results are very close, although the non-linear modes will be changed.

Table 4. Comparison of the results obtained by the model created for an isotropic material with recent scientific work in the same context., where (***E = 1 GPa*** ;***v=0.3***) and the geometric parameters (***t=1;e=1×t;L=10t***).

$\hbar = \frac{L}{t}$.	Nonlocal parameter (n) (m=100)	The dimensionless deflection $\overline{\overline{Z_{adm}}}$	
		(Sayyad & Ghugal, 2021)	**Present**
5	0	1.4347	**1.4433**
	1	1.5716	**1.5647**
	2	1.7045	**1.7123**
	3	1.8415	**1.8479**
	4	1.9804	**1.9861**
10	0	1.3394	**1.3394**
	1	1.4675	**1.4655**
	2	1.5956	**1.5983**
	3	1.7237	**1.7364**
	4	1.8517	**1.8520**
20	0	1.3134	**1.3132**
	1	1.4406	**1.4418**
	2	1.5637	**1.5638**
	3	1.6919	**1.6920**
	4	1.8161	**1.8121**
100	0	1.3036	**1.3035**
	1	1.4301	**1.4308**
	2	1.5567	**1.5547**
	3	1.6802	**1.6806**
	4	1.8047	**1.8055**

We begin the study with our new materials, plaster reinforced with DISS nano-short fibres. The deflection will be calculated for the different volume fractions of the nano-short fibres by the effective properties of the materials (Plaster + DISS Algerian).

From **Tables 3 and 4**, if the ratio between the length and thickness of the beam changes, the deflection decreases; on the other hand, if we fix the recent ratio and the modes of the non-linear parameter (**n**) increase such that (**m=100**), the deflection of the beam decreases.

The results are presented in **Table 5** (The cross-section is a square **t=e**). The deflection decreases when the section is created if the length ratio is along the length of the beam. For this, the results are logical.

In **Tables 6, 7, and 8**, successively and alternately, we vary the cross-section **e = {1;0.75;0.5;0.25}×t**; with a geometric relationship that also varies between the beam length and the thickness.

If the section becomes rectangular on the semi-axis [oy), the transverse section becomes rectangular automatically; the inertia will change, then the arrow increases, and the opposite is correct.

So, it is better to have the thickness reversed so the beam is more resistant to gains in inertia.

Table 5. Comparison of the results obtained by the model created for an isotropic material with recent scientific work in the same context. Where (***E=E(V%) GPa*** ; ***v=v(V%)***) and the geometric parameters (***t=1;e=1×t;L=ℏ ×t***).

$\hbar = \frac{L}{t}$.	Nonlocal parameter (**n**) (**m=100**)	The dimensionless deflection $\overline{\overline{Z}}_{adm}$						
		V(00%)	V(05%)	V(10%)	V(15%)	V(20%)	V(25%)	V(30%)
5	0	1.0164	1.0803	1.1528	1.2357	1.3314	1.4433	0.9596
	1	1.1019	1.1712	1.2497	1.3396	1.4434	1.5647	1.0403
	2	1.2059	1.2817	1.3677	1.4660	1.5796	1.7123	1.1385
	3	1.3014	1.3832	1.4760	1.5821	1.7047	1.8479	1.2287
	4	1.3987	1.4866	1.5863	1.7004	1.8322	1.9861	1.3205
10	0	0.9432	1.0025	1.0698	1.1467	1.2356	1.3394	0.8905
	1	1.0321	1.0970	1.1706	1.2547	1.3520	1.4655	0.9744
	2	1.1256	1.1964	1.2766	1.3684	1.4745	1.5983	1.0627
	3	1.2228	1.2997	1.3869	1.4866	1.6018	1.7364	1.1545
	4	1.3042	1.3862	1.4792	1.5856	1.7085	1.8520	1.2314
20	0	0.9248	0.9829	1.0489	1.1243	1.2115	1.3132	0.8731
	1	1.0154	1.0792	1.1516	1.2344	1.3301	1.4418	0.9587
	2	1.1013	1.1705	1.2491	1.3389	1.4427	1.5638	1.0398
	3	1.1915	1.2664	1.3514	1.4486	1.5609	1.6920	1.1250
	4	1.2762	1.3564	1.4474	1.5515	1.6717	1.8121	1.2049
100	0	0.9179	0.9757	1.0411	1.1160	1.2025	1.3035	0.8667
	1	1.0076	1.0710	1.1428	1.2250	1.3199	1.4308	0.9513
	2	1.0948	1.1637	1.2417	1.3311	1.4342	1.5547	1.0337
	3	1.1835	1.2579	1.3423	1.4388	1.5503	1.6806	1.1174
	4	1.2715	1.3515	1.4421	1.5458	1.6656	1.8055	1.2005

The non-dimensional deflection is presented in **Figure 2**; the tracing of the latter is correct because the beam is supported, and the maximum deflection is in the middle of the beam.

Therefore, if the volume fraction (**V%**) of Algerian DISS increases, the deflection will be less each time with an increase of **5%**. The best results are **30%**. We remind you that stopping at **30%** of nano-short fibres is required because the reinforcement is an organic material, and we can go further with the fractions we limit ourselves to **30%.**

In this part of the diagnosis of the results of **Figure 2**, the stress depends on the bending moment of this reason in the elasticity level. If Young's modulus increases, the resistance will be better, and the deflection will return more minor.

DISS Algerian nano-fibres become more efficient in reducing deflection along the semi-axis [**oz**). Therefore, this reinforcement is perfect for reinforcing plaster.

The improvement between the ordinary dry plaster and the plaster with a fraction of **30%** we have is a reduction of 42% in the deflection, which presents the importance of this reinforcement. The significant reduction in deflection (42%) achieved with a 30% addition of fibres underscores the practical value of the proposed material. The experimental and theoretical results are consistent and well-illustrated. The mathematical model based on recognized theories (HSDT, Piggot) is a significant strength. The validations with comparative data demonstrate consistency with both theoretical and experimental results.

Table 6. Comparison of the results obtained by the model created for an isotropic material with recent scientific work in the same context., where (***E=E(V%) GPa***; ***v= v(V%)***) and the geometric parameters (***t=1;e=0.75×t;L=ℏ ×t***).

$\hbar = \frac{L}{t}$.	Nonlocal parameter (n) (m=100)	The dimensionless deflection $\overline{\overline{Z_{adm}}}$						
		V(00%)	V(05%)	V(10%)	V(15%)	V(20%)	V(25%)	V(30%)
5	0	1.4433	1.3314	1.2357	1.1528	1.0803	1.0164	0.9596
	1	1.5647	1.4434	1.3396	1.2497	1.1712	1.1019	1.0403
	2	1.7123	1.5796	1.4660	1.3677	1.2817	1.2059	1.1385
	3	1.8479	1.7047	1.5821	1.4760	1.3832	1.3014	1.2287
	4	1.9861	1.8322	1.7004	1.5863	1.4866	1.3987	1.3205
10	0	1.3394	1.2356	1.2357	1.0698	1.0025	0.9432	0.8905
	1	1.4655	1.3520	1.3396	1.1706	1.0970	1.0321	0.9744
	2	1.5983	1.4745	1.4660	1.2766	1.1964	1.1256	1.0627
	3	1.7364	1.6018	1.5821	1.3869	1.2997	1.2228	1.1545
	4	1.8520	1.7085	1.7004	1.4792	1.3862	1.3042	1.2314
20	0	1.3132	1.2115	1.1243	1.0489	0.9829	0.9248	0.8731
	1	1.4418	1.3301	1.2344	1.1516	1.0792	1.0154	0.9587
	2	1.5638	1.4427	1.3389	1.2491	1.1705	1.1013	1.0398
	3	1.6920	1.5609	1.4486	1.3514	1.2664	1.1915	1.1250
	4	1.8121	1.6717	1.5515	1.4474	1.3564	1.2762	1.2049
100	0	1.3035	1.2025	1.1243	1.0411	0.9757	0.9179	0.8667
	1	1.4308	1.3199	1.2344	1.1428	1.0710	1.0076	0.9513
	2	1.5547	1.4342	1.3389	1.2417	1.1637	1.0948	1.0337
	3	1.6806	1.5503	1.4486	1.3423	1.2579	1.1835	1.1174
	4	1.8055	1.6656	1.5515	1.4421	1.3515	1.2715	1.2005

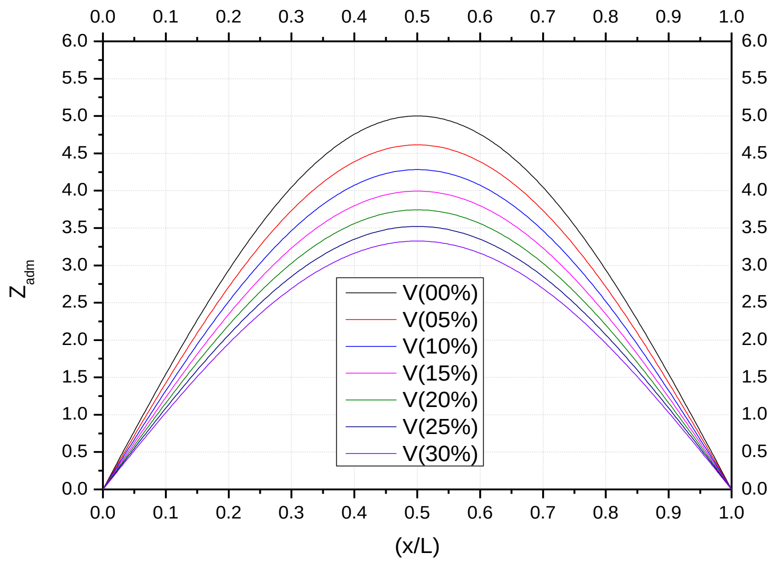

Figure 2. The deflection $\overline{\overline{Z_{adm}}}$ for the different volume fractions is **V(%)** or the following geometrics parameters **(t=1;e=1×t;L= 5×t)**

Table 7. Comparison of the results obtained by the model created for an isotropic material with recent scientific work in the same context. where (***E=E(V%) GPa*** ; ***v=v(V%)***) and the geometric parameters (***t=1;e=0.5×t;L=ℏ×t***).

$\hbar = \frac{L}{t}$.	Nonlocal parameter (**n**) (**m=100**)	The dimensionless deflection $\overline{\overline{Z}}_{adm}$						
		V(00%)	V(05%)	V(10%)	V(15%)	V(20%)	V(25%)	V(30%)
5	0	1.4433	1.3314	1.2357	1.1528	1.0803	1.0164	0.9596
	1	1.5647	1.4434	1.3396	1.2497	1.1712	1.1019	1.0403
	2	1.7123	1.5796	1.4660	1.3677	1.2817	1.2059	1.1385
	3	1.8479	1.7047	1.5821	1.4760	1.3832	1.3014	1.2287
	4	1.9861	1.8322	1.7004	1.5863	1.4866	1.3987	1.3205
10	0	1.3394	1.2356	1.1467	1.0698	1.0025	0.9432	0.8905
	1	1.4655	1.3520	1.2547	1.1706	1.0970	1.0321	0.9744
	2	1.5983	1.4745	1.3684	1.2766	1.1964	1.1256	1.0627
	3	1.7364	1.6018	1.4866	1.3869	1.2997	1.2228	1.1545
	4	1.8520	1.7085	1.5856	1.4792	1.3862	1.3042	1.2314
20	0	1.3132	1.2115	1.1243	1.0489	0.9829	0.9248	0.8731
	1	1.4418	1.3301	1.2344	1.1516	1.0792	1.0154	0.9587
	2	1.5638	1.4427	1.3389	1.2491	1.1705	1.1013	1.0398
	3	1.6920	1.5609	1.4486	1.3514	1.2664	1.1915	1.1250
	4	1.8121	1.6717	1.5515	1.4474	1.3564	1.2762	1.2049
100	0	1.3035	1.2025	1.1160	1.0411	0.9757	0.9179	0.8667
	1	1.4308	1.3199	1.2250	1.1428	1.0710	1.0076	0.9513
	2	1.5547	1.4342	1.3311	1.2417	1.1637	1.0948	1.0337
	3	1.6806	1.5503	1.4388	1.3423	1.2579	1.1835	1.1174
	4	1.8055	1.6656	1.5458	1.4421	1.3515	1.2715	1.2005

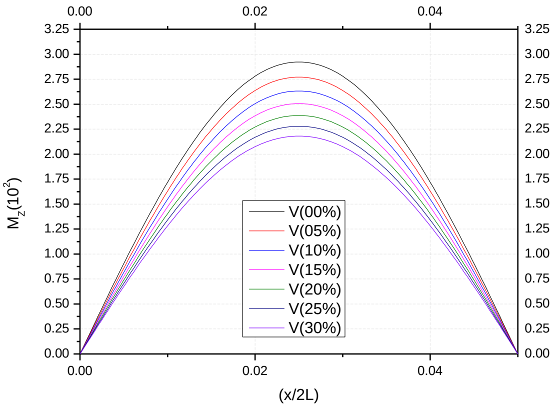

Figure 3. The pure bending **Mz** for the different volume fractions is **V (%)** or the following geometrics parameters **(t=1; e=1×t; L= 10×t)**

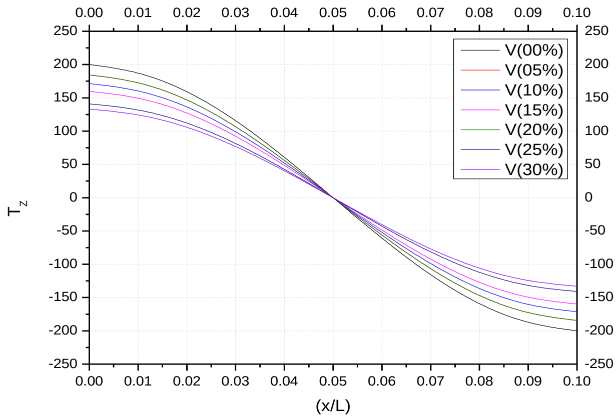

Figure 4. The pure shear force **Tz** for the different volume fractions is **V (%)** or the following geometrics parameters **(t=1; e=1×t; L= 10×t)**

Table 8. Comparison of the results obtained by the model created for an isotropic material with recent scientific work in the same context., where (***E=E(V%) GPa***; v= ***v(V%)***) and the geometric parameters (***t=1; e=0.25×t;L=*** $\hbar$ ***×t***).

$\hbar = \frac{L}{t}$.	Nonlocal parameter (n) (m=100)	The dimensionless deflection $\overline{\overline{Z_{adm}}}$						
		V (00%)	V (05%)	V (10%)	V (15%)	V (20%)	V (25%)	V (30%)
5	0	1.4433	1.3314	1.2357	1.1528	1.0803	1.0164	0.9596
	1	1.5647	1.4434	1.3396	1.2497	1.1712	1.1019	1.0403
	2	1.7123	1.5796	1.4660	1.3677	1.2817	1.2059	1.1385
	3	1.8479	1.7047	1.5821	1.4760	1.3832	1.3014	1.2287
	4	1.9861	1.8322	1.7004	1.5863	1.4866	1.3987	1.3205
10	0	1.3394	1.2356	1.1467	1.0698	1.0025	0.9432	0.8905
	1	1.4655	1.3520	1.2547	1.1706	1.0970	1.0321	0.9744
	2	1.5983	1.4745	1.3684	1.2766	1.1964	1.1256	1.0627
	3	1.7364	1.6018	1.4866	1.3869	1.2997	1.2228	1.1545
	4	1.8520	1.7085	1.5856	1.4792	1.3862	1.3042	1.2314
20	0	1.3132	1.2115	1.1243	1.0489	0.9829	0.9248	0.8731
	1	1.4418	1.3301	1.2344	1.1516	1.0792	1.0154	0.9587
	2	1.5638	1.4427	1.3389	1.2491	1.1705	1.1013	1.0398
	3	1.6920	1.5609	1.4486	1.3514	1.2664	1.1915	1.1250
	4	1.8121	1.6717	1.5515	1.4474	1.3564	1.2762	1.2049
100	0	1.3035	1.2025	1.1160	1.0411	0.9757	0.9179	0.8667
	1	1.4308	1.3199	1.2250	1.1428	1.0710	1.0076	0.9513
	2	1.5547	1.4342	1.3311	1.2417	1.1637	1.0948	1.0337
	3	1.6806	1.5503	1.4388	1.3423	1.2579	1.1835	1.1174
	4	1.8055	1.6656	1.5458	1.4421	1.3515	1.2715	1.2005

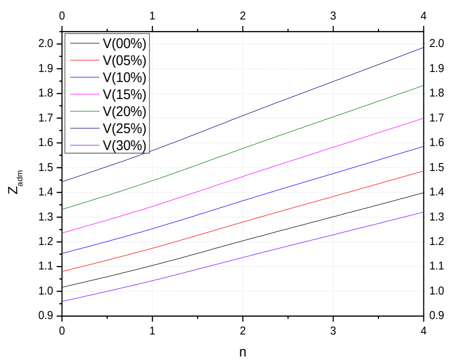

(A) : (t=1 ; e=1×t ; L= 5×t)

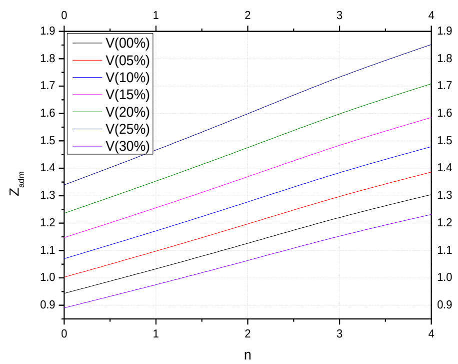

(B) : (t=1 ; e=1×t ; L= 10×t)

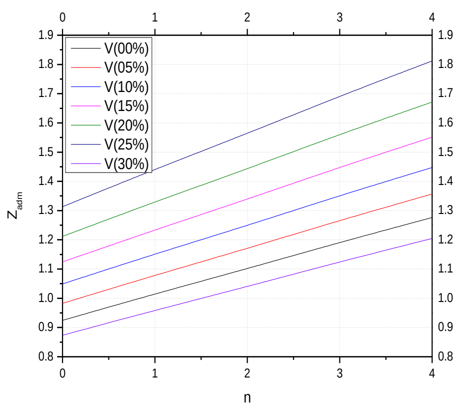

(C) : (t=1 ; e=1×t ; L= 20×t)

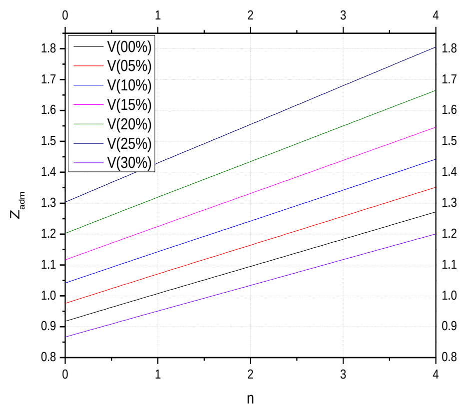

(D) : (t=1 ; e=1×t ; L= 100×t)

Figure 5. The deflection for all four non-local parameters **(n=0;1;2;3;4)** for the different volume fractions is **V (%). {A, B, C, D}**

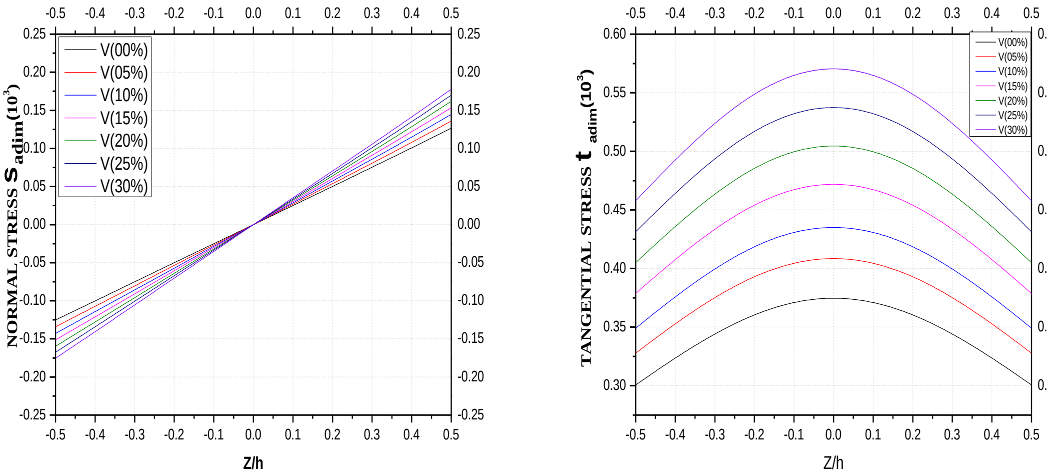

(A) Normal stress **(B): Tangential stress**

Figure 6. The deflection for all four non-local parameters **(n=0;1;2;3;4)** for the different volume fractions is **V (%). {A, B, C, D}**

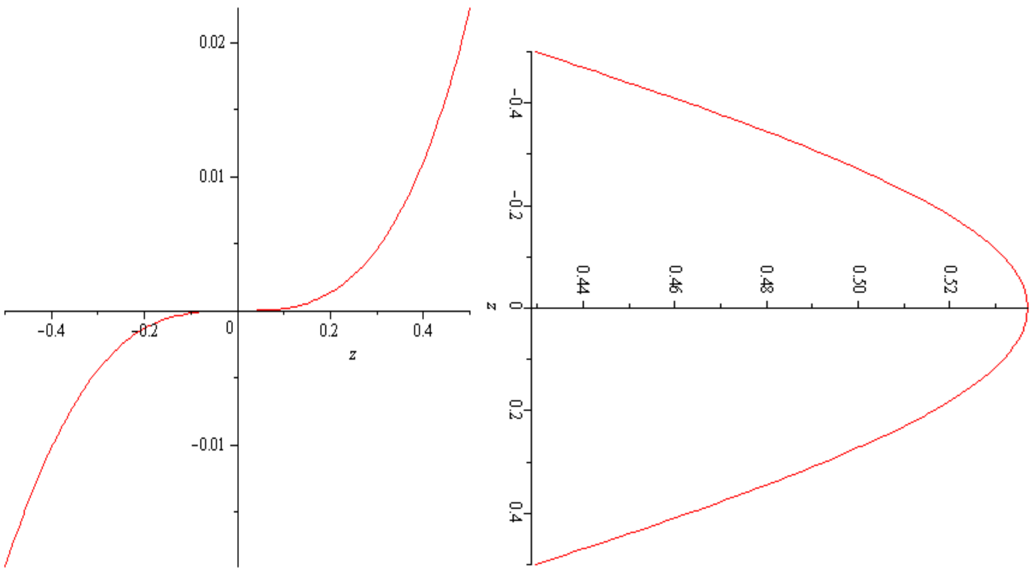

(A) Function of Normal stress **(B) Function of Tangential stress** $\left[-\frac{h}{2}..\frac{h}{2}\right]$

Figure 7. The Plotting of the function of the normal stress and the tangential stress in the interval $\left[-\frac{h}{2}..\frac{h}{2}\right]$ are presented in the two graphs **{A, B}**

We base ourselves on basic mathematical books to determine the new functions and estimate the shear under a hyperbolic function, and also for the development of calculation models, among its references (TAHA SOSHY) (Sochi, 2022); (Wihlem Flugges) (Flügge, 1972). In **Figure 3**, it is always noted that the weighting relationship between the bending and the stress in the elasticity of the bending moment is the greatest in the case where (**V%=0%**), the greatest is considered in the middle of the arrow. The lowest is (**V%=30%**), so these reinforcements work perfectly to reduce the bending moment of this type of beam.
In this part of the diagnosis of the results of **Figure 2**, the stress depends on the bending moment of this reason in the elasticity level. If Young's modulus increases, the resistance will be better, and the deflection will return more minor. Since the maximum value of the stress is at the middle of the beam, we notice that the cutting force is zero in the middle of the beam and maximum at the limited once by a negative value and the second time by a positive value, and increasing the reinforcement reduces the value of the shear force. The difference in the shear force of an ordinary plaster beam and a plaster reinforced in 30% by DISS nano-fibres is of a value of 38%. In all graphs {**A, B, C,** and **D**}, the **30%** gives the least tracing in all cases in variation of the

geometry of the beams. The deflection increases as a function of change in nonlinearity (the parameter non-local) (**n**), and the deflection increases as a function of the non-locality of the beam. What shows up in **Figure 4**. Graph A of **Figure 5** shows that the everyday stress increases on the variation in the thickness (z) and will become (**zero**) in the middle of the beam in the transverse section because of the central core and, in turn, the neutral axis. While either the extremity or **z=-h/2** or **z=h/2** the shear force is low, the best results or **z=0** are displayed in graph (**B**) of **Figure 5**. Concerning the volume of the fraction, as always, the reinforcement chosen works perfectly in the case of bending. The plots of the two functions, A for the usual stresses and **B** for the shear stresses, as shown in **Figure 6**, clearly illustrate tensile and compressive stresses. Consequently, a parabolic shear force is depicted, which reaches its optimal value at **z=0.** These two graphs represent the standards of material strength and plane elasticity. $(\tau = 0 \rightarrow \sigma^{\max})$; $(\sigma = 0 \rightarrow \tau^{\max})$. The work method is purely theoretical; the effective method involves randomly mixing gypsum with Algerian fibre courses. This study was conducted under static conditions, and future studies will incorporate the effects of hygrothermal conditions and climate change. The maximum allowable volume fraction for organic materials is limited to 30% for safety reasons. It is noted that several constructions have been carried out using this technique. This method can be used in concrete structures for acoustic and thermal applications.

4. Conclusion

At the end of this work, we conclude the following:

1- The non-local parameter (n) increases the deflection of the beam in all cases.

2-The geometrical relationships influence the beams' deflection; the best choice is the rectangular beam based on its base or a square section.

3-Increasing the volume fraction of nano-short fibres reduces deflection and improves the resistance of plaster against bending.

4-The nano-short fibres of DDIIS designed as plant material (biomaterials) have positive results in improving the properties of plasters.

5-The laws developed to function as improved HSDT, which can be used for verification and homogenization by biological materials.

6-This paper is important because it combines two heterogeneous materials and two different mineral and biological sources, opening a broad vision in research into innovative materials. After all, we can go up to 30% by biological reinforcements.

7-Biomaterials are renewable resources that have never been replenished, which can reinforce construction materials in civil engineering.

8- This new plaster can be used in architectural aesthetics, reinforcing old buildings and rehabilitating old mosques and churches built using plaster.

9-It is also demonstrated that this new mathematical model can calculate the bending of beams using HSDT.

10-The improved homogenization model can be used as a reference for combined hydraulic binders and short organic nano-fibres.

11- The impact of using these fibres in construction is to improve the socioeconomic sector by promoting and enhancing the value of this type of material in building applications for declared objectives.

12- The role of fibres in construction materials is primarily to reduce thermal conductivity and enhance acoustic insulation.

Conflict of Interest

On behalf of all authors, the corresponding author states that there is no conflict of interest.

Data Availability

No data was used for the research described in the article.

List of Abbreviations

ζ_d : The ratio between the maximum fibre diameter and the particles diameters of the ultimate plaster grains;
$\hat{\lambda}_l$: The ratio between the maximum fibre length and the minimum length fibre of the reinforcing fibers;
$E_{\text{hom}}^{P\&D}$: Young's Modulus homogeneous;
$E_P ; E_D$: The Young's Modulus of Plaster and the DISS respectively;
$\upsilon_{\text{hom}}^{P\&D} ; \nu_P ; \nu_D$: The Poisson ratio homogeneous, Plaster and the DISS respectively ;
V_D : Volume fraction ;
$G_{\text{hom}}^{P\&D}$: shear modulus;
$\overline{X}$ and $\overline{Z}$: The Poisson ratio homogeneous, Plaster and the DISS respectively axial and transverse displacement respectively in x and z directions ;
ψ : The shear slope;
$\overline{x_0}$ and $\overline{z_0}$: The displacement in any position;
$\overline{\overline{Z_{adm}}}$: The dimensionless deflection;
Ω_x : The normal deformation (in x-axis);
$\wp_{xz}$: The transverse deformation (in two axis x,y);
$\chi(z)$: Function representative of shear deformation;
$\delta(z)$: One minus first derivation of function representative shear deformation;
ψ : Rotation;
$\wp_{xz}^0$: first deformation produces buy rotation;
Ω_x^0 : first displacement;
$\wp_{xz}^0$: first distortion;
P_x^b : normal deformation in beam;
P_x^s : Distortion produce buy the shear deformation;
σ_x : The bending of a beam;
τ_{xz} : The normal and the tangential stress are as follows;
$E_{\text{hom}}^{P\&D}$ and $\upsilon_{\text{hom}}^{P\&D}$: The elastic modulus and Poisson's ratio of a homogeneous plaster beam reinforced by short DISSS fibers are determined after homogenization as an isotropic beam;
(**d$_i$**) : The initial during;
(**d$_f$**): The final during ;
P: Potential energy;
H: Kinetic energy;
$\Upsilon(x)$: The loading applied to the beam studied;
$(F_r^x ; M_r^b ; M_r^s ; \Re^{'})$: The resulting forces and moments ;
(z= { $-\frac{t}{2}$ to $\frac{t}{2}$ }) : The thickness ;
$(\bar{A}_{st} ; \bar{B}_{st} ; \bar{C}_{st} ; \bar{D}_{st} ; \bar{E}_{st} ; \bar{F}_{st} ; \bar{G}_{st})$: The stiffness coefficients;
e: Nonlinear parametrium;
δ : Variation ;
[**K$_r$**] : The rigidity matrix ;
{**U$_d$**}: The displacement vector ;
{**P$_r$**} : The force vector ;
(**œ**): The parameter non-local cogent the characteristics of materials used in analyses ;
$\Delta_{error(\%)}$: Variation error;
V(%) : Volume fraction ;
$\hbar$: Parameter length devise by thicknessm;
m, n : buckling Mods.

References

Abdullah, A., & Sichani, E. F. (2009). Experimental study of attenuation coefficient of ultrasonic waves in concrete and plaster. *The International Journal of Advanced Manufacturing Technology*, *44*, 421-427.

Ali, F. A., Abd-Allah, H. H., & Mari, B. H. (2015). Improvement of the physical, mechanical and thermal insulation properties to produce gypsum boards by using waste materials. *Iraqi Journal of Science*, 1972-1982.

Arbabi, F. (1991). Structural analysis and behavior. *(No Title)*.

Berenger, A., Olivier, G., Lanos, C., Daiguebonne, C., Freslon, S., Tessier, C., Laurans, M., Baux, C., & Greffet, H. (2015). A new calcium sulfate-based plaster composed of composite particles. *Materials and structures*, *48*, 2685-2696.

Boukert, B., Benkhedda, A., Adda, E., & Khodjet-Kesba, M. (2019). Hygrothermal stresses analysis of thick composite plates using high order theory under a Fick concentration distribution. *Procedia Structural Integrity*, *17*, 37-43.

de Bilbao, E., Blond, E., Michel, C., Cutard, T., Schmitt, N., & Poirier, J. (2010). A new method to Determine the Young's Modulus of Refractory Materials. *Interceram*, *59*(1), 34-38.

Fahih, K. J., Alkaysi, O. A., & Abelkhalek, L. S. (2005). The Effect of some Natural Admixtures on the setting Time of Iraqi Plaster of Parts. *Engineering and Technology Journal*, *24*(9).

Flügge, W. (1972). *Tensor analysis and continuum mechanics*. Springer.

Jamalzadeh, N., Heidary, S., Zare, Y., & Rhee, K. Y. (2018). A multistep methodology based on developed Takayanagi, Paul and Ouali models for tensile modulus of polymer/carbon nanotubes nanocomposites above percolation threshold assuming the contribution of interphase regions. *Polymer Testing*, *69*, 1-8.

Karni, J., & Karni, E. Y. (1995). Gypsum in construction: origin and properties. *Materials and structures*, *28*, 92-100.

Merzoud, M., & Habita, M. (2008). Elaboration de composite cimentaire à base de diss «Ampelodesma Mauritanica». *Afrique science: Revue internationale des sciences et technologie*, *4*(2).

Mohammed, L., Ansari, M. N., Pua, G., Jawaid, M., & Islam, M. S. (2015). A review on natural fiber reinforced polymer composite and its applications. *International journal of polymer science*, *2015*(1), 243947.

Mohammed, M. (2010). Residual Compressive Strength of Iraqi-Gypsum Subjected to Elevated Temperature Exposure". *Journal of Babylon University/Pure and Applied Sciences/No*, *5*.

Piggott, M. (1981). A theoretical framework for the compressive properties of aligned fibre composites. *Journal of materials science*, *16*, 2837-2845.

Piggott, M. (2002). *Load bearing fibre composites*. Springer Science & Business Media.

Rahimzadeh, C. Y., Mohammed, A. S., & Barzinjy, A. A. (2022). Microstructure characterizations, thermal analysis, and compression stress–strain behavior of lime-based plaster. *Construction and Building Materials*, *350*, 128921.

Rinaldi, M., Bragaglia, M., & Nanni, F. (2023). Mechanical performance of 3D printed polyether-ether-ketone nanocomposites: An experimental and analytic approach. *Composite Structures*, *305*, 116459.

Saurav, S., & Porter, I. (2018). Numerical Modelling of Polymer Coated Plaster Beams. ISRM International Symposium-Asian Rock Mechanics Symposium,

Sayyad, A. S., & Ghugal, Y. M. (2021). Bending, buckling, and vibration analysis of functionally graded nanobeams using an inverse trigonometric beam theory. *International Journal of Nano Dimension*, *12*(2), 164-174.

Sayyad, A. S., Hadji, L., & Tounsi, A. (2023). On the mechanics of FG nanobeams: a review with numerical analysis. *Forces in Mechanics*, 100219.

Sochi, T. (2022). *Principles of Tensor Calculus*. Taha Sochi.

Timoshenko, S. P., & Gere, J. M. (2012). *Theory of elastic stability*. Courier Corporation.

Touam, L., & Derfouf, S. (2021). Effect of the Varying Percentage Diss Fiber on Mechanical Behaviour of the Based Polyester Bio-Composite. *Journal of Composite & Advanced Materials/Revue des Composites et des Matériaux Avancés*, *31*(3).

Wadee, A., Achanta, P., Walker, P., McCullen, N., & Ferrandiz-Mas, V. (2023). Novel gypsum based plasters with phase change material impregnated lightweight aggregates for energy efficient retrofitting. *Construction and Building Materials*, *403*, 133159.

Wang, L., Cao, M., Li, X., Du, W., & Wang, X. (2023). A novel approach for improving the water resistance of gypsum plaster by internal mixing hypromellose and external coating waterproofing agent. *Construction and Building Materials*, *401*, 132940.

Yaqoob, W. M. (2019). Characteristics of Artificial, Gypsified and Natural Gypseous Soils under Dry Condition. *Engineering and Technology Journal*, *37*(8 Part A).

Zare, Y., & Rhee, K. Y. (2020). Development of expanded takayanagi model for tensile modulus of carbon nanotubes reinforced nanocomposites assuming interphase regions surrounding the dispersed and networked nanoparticles. *Polymers*, *12*(1), 233.